IEIE Transactions on Smart Processing and Computing, vol. 9, no. 5, October 2020
https://doi.org/10.5573/IEIESPC.2020.9.5.353

Improving the Contrast of Aerial Images using a New Multi-concept Algorithm

Zohair Al-Ameen

Department of Computer Science, College of Computer Science and Mathematics, University of Mosul / Nineveh, Iraq
qizohair@uomosul.edu.iq

Received October 20, 2019; Revised March 26, 2020; Accepted April 16, 2020; Published October 30, 2020

** Regular Paper*

***Abstract*:** Aerial images are highly beneficial for a range of real-life applications. On the other hand, the quality of these images is often degraded by a low-contrast effect caused by many causatives that are difficult to avoid during the acquisition process. Therefore, a new multi-concept algorithm is proposed to improve the contrast of aerial images adequately in a fully automatic way. The proposed algorithm combines several processing concepts of S-curve mapping functions, logarithmic image processing, and normalization. The newly developed algorithm was tested with artificial and natural-degraded images, and the quality of the resulting images from different comparisons was evaluated using four advanced image quality assessment (IQA) metrics. Intensive experiments and evaluations showed that the proposed algorithm could improve the contrast for various types of aerial images rapidly. In addition, it could outperform many advanced contrast enhancement algorithms regarding the IQA scores, perceived quality, and processing speed.

***Keywords*:** Aerial imaging, Contrast enhancement, Multi-concept algorithm, Remote sensing

1. Introduction

Aerial photography is the process of capturing images from the air and is deemed an essential field for remote sensing. In this process, the Earth's surface is photographed using highly accurate cameras that can be mounted on airplanes, balloons, drones, helicopters, kites, and rockets [1]. Aerial photography produces beneficial images that are used in archaeology, cartography, conveyancing, commercial advertising, environmental studies, land-use planning, and movie production [2]. Despite the major advantages of aerial images, they are often degraded by low-contrast effect [3] caused by imperfect atmospheric conditions and limitations in the imaging system [4]. In addition, high-end aerial image acquisition units often fail to capture adequate quality images under certain situations [5]. Owing to the increasing demand for clearer aerial images, it is essential to process the low-contrast effect properly to produce images with better visual details [6]. Therefore, many contrast enhancement algorithms have been developed to deal with this degradation. In this context, this paper reviewed two types of contrast enhancement algorithms.

The first type included the following algorithms developed specifically for aerial and remote sensing images: wavelet-based nonlinear image enhancement (WBNIE) [7], singular value decomposition and discrete wavelet transform (SVD_DWT) [8], integrated framework for aerial image restoration (IFAIR) [9], and regularized-histogram equalization and discrete cosine transform (RHEDCT) [10]. The second type included the following algorithms, which were developed for usual images and applied to aerial images: brightness preserving dynamic fuzzy histogram equalization (BPDFHE) [11], exposure-based sub-image histogram equalization (ESIHE) [12], median-mean based sub-image-clipped histogram equalization (MMSICHE) [13], histogram specification approach (HSA) [14], and histogram equalization with maximum intensity coverage (HEMIC) [15].

A previous study developed a wavelet-based algorithm that can improve the contrast in a nonlinear fashion [7]. This algorithm included three distinct stages. The first and the last stages were implemented in the spatial domain, whereas the second stage was implemented in the discrete wavelet domain. The first stage involved the application of histogram adjustment based on the behavior of human vision. The second step involved the use of local contrast adjustment and dynamic range compression in the wavelet domain. In contrast, the last step involved the utilization of a specialized color restoration process to improve the colors of the resulting image. Similarly, an enhancement algorithm that depends on the concepts of singular value

decomposition (SVD) and discrete wavelet transform (DWT) was introduced [8]. This algorithm starts by decomposing the inputted image into four frequency sub-bands by applying the DWT. An approximation of the singular value matrix at the low-low subband was made. Finally, an inverse DWT was applied to reconstruct the image subbands and produce the final image.

In addition, an integrated enhancement framework consisting of three distinct steps was proposed [9]. The first step included the application of a color balancing technique by determining the mean intensities for each color channel. The second step included the utilization of saturation improvement using shift and scale operations. The last step included the application of contrast enhancement depending on the information of the detected edges. The output obtained from this step was considered the final result. An algorithm that applies a regularized version of histogram equalization for global contrast enhancement was introduced [10]. Regularization was achieved using both the sigmoid function and histogram features to derive a distribution function that could be used to produce a globally-enhanced image using a specific lookup table. Next, the coefficients of the discrete cosine transform for the globally enhanced image were fine-tuned automatically to provide further enhancements for the local details of the image.

A fuzzy-based algorithm that starts by calculating the fuzzy histogram of the input image was developed [11]. The determined histogram was partitioned into multiple sub-histograms using local maxima. A dynamic histogram equalization procedure was then applied to each sub-histogram using a special spanning function that depends on the pixel's tonality. Finally, the resulting image was obtained by normalizing the overall brightness. For color images, this algorithm performed its operations using the YCbCr color space. In addition, an algorithm was designed to calculate the different exposure thresholds that can be used to partition the input image into multiple sub-images [12]. The histogram of each sub-image was then clipped using a specialized threshold value that was determined automatically based on the average of the existing grey levels to adjust the enhancement rate. The histogram of each sub-image was equalized separately, and all the processed sub-images were combined to form the final resulting image.

Similarly, a histogram-based algorithm that includes several distinct steps was introduced [13]. The first step involved a calculation of the mean and median brightness values for the input image. The second step involved a histogram clipping process via the utilization of a plateau limit as the intensity median. The third step involved the equalization of each sub-image. All the processed sub-images were integrated to obtain the result. In addition, a histogram specification-based algorithm was proposed to convert the RGB color image to the hue, saturation, and intensity (HSI) domain [14]. The mean image brightness was calculated, and an adopted histogram specification strategy was implemented to improve the contrast, produce image brightness similar to the original image, and attenuate the over-enhancement artifacts without affecting the colors or saturation. A specialized histogram equalization procedure was then applied based on the determined histogram specification strategy. The output of this step was converted back to the RGB color domain to produce the final image.

A histogram-based algorithm that works by performing a magnitude stretch operation on the RGB color image and converting it to an HSI color domain was developed [15]. A histogram equalization approach was then applied to the I channel of the pre-processed image. Based on the output of this step, the empty bins of the histogram were detected, the entropy was calculated, and a special objective function was implemented recursively to allow maximum coverage of the intensity range. Finally, the image was converted back to the RGB color domain to obtain the final resulting image. In the past few years, deep learning (DL) has been utilized for color image enhancement [36]. DL is a learning method that belongs to a division of a larger family of machine learning approaches that depend on artificial neural networks to produce results that are as good as or better than the performance of human experts. A DL based method using some standard image processing methods was introduced to derive certain derivative maps [37]. A deep decomposition network was then implemented along with end-to-end training to obtain the illumination features and determine the relationship between normal and low-illumination. Finally, a deep improvement network was used to obtain the final result.

As seen from the algorithms reviewed, different ideas have been utilized for contrast enhancement. The most complicated are those related to DL because of their high computation cost, and the many variables involved that cannot be determined properly by the normal user. Still, the chances for improving or producing new algorithms for aerial image enhancement are high, and the likelihood of doing so remains wide open. Therefore, this paper proposes a new fully automatic multi-concept algorithm to improve the contrast of aerial images depending on a combination of several processing concepts of the S-curve mapping functions, logarithmic image processing, and normalization. Many S-curve functions can be used for contrast enhancement [16]. S-curve functions work by adjusting the pixel values of a given image according to the X and Y relationship defined by the function [17]. Moreover, there are many types of S-curve functions, in which a simple function may not be appropriate for all types of images [18]. In addition, the use of a single function may not be sufficient for proper contrast enhancement [16]. Therefore, it is possible to combine several S-curve functions to obtain results with better tonality [19].

In addition, logarithmic image processing (LIP) methods are used extensively in the field of contrast enhancement [20]. Similarly, different LIP methods exist that can combine the characteristics of two images to produce a better quality image. Normalization is another method that is widely used to fit the image intensities to the usual dynamic range [21]. The proposed algorithm was tested with both artificial and natural degraded low-contrast, and compared with nine specialized contrast enhancement algorithms. Moreover, the comparison results were evaluated using four advanced image quality

assessment (IQA) metrics. The results obtained by intensive comparisons and experiments showed that the proposed algorithm has promising processing abilities, and can outperform many advanced contrast enhancement algorithms in recovering acceptable quality results from their low-contrast counterparts. The remainder of the article is arranged as follows. Section 2 describes the proposed algorithm in detail, and Section 3 reports the results and their related discussions. Finally, a brief conclusion is given in Section 4.

2. Proposed Algorithm

The proposed multi-concept algorithm was developed based on the utilization of multiple processing concepts. The design of this algorithm was driven by two motivations. The first was the recovery of acceptable quality results from the degraded counterpart without generating visible flaws in a fully automatic manner. The second was the design of a low-complexity algorithm that could produce high-quality results. In general, the S-curve mapping functions are useful in improving the contrast of various digital images [22]. The application of many of these functions introduced noticeable tonal enhancements [19]. In the proposed algorithm, however, several S-curve functions were used for tonality enhancement. In addition, logarithmic image processing was used to combine the outcomes of two S-curve functions. In contrast, the normalization function was used to accommodate image intensities to the standard dynamic range. The appropriate S-curve functions were selected by conducting intensive experiments on various well-known functions. In particular, the proposed algorithm started by applying the cumulative distribution function of a generalized logistic distribution Type-II (CDF-GLD-II). This function is one type of S-curve function that can provide a well-regulated tonal alteration. The CDF-GLD-II function was calculated using Eq. (1) [23].

$$I_1 = 1 - \left(\frac{\exp(-\lambda X)}{\left(1+\exp(-X)\right)^{\lambda}} \right) \tag{1}$$

where I_1 is the resulting image from the CDF-GLD-II function; X is the input color image in RGB form, in which its intensities are transformed to the range of (0 to 1). The main reason for doing so is that the mathematical equations used in this algorithm require the input to be in such form to deliver the desired results. If the range used is 0 to 255, the intensities would be out of this range after being processed, and the results would appear simply as white images. On the other hand, λ is a parameter that is used to control the level of tonal alteration, in which it should fulfill $\lambda > 0$. Generally, intensive experiments on hundreds of images showed that images with acceptable brightness and contrast could be obtained when λ was in the range of (1 to 1.4). The best results were obtained when λ = 1.2. Therefore, λ was set to 1.2 for all experiments and comparisons. Next, the input RGB color image X was processed by another S-curve function, which is the hyperbolic tangent (HT) function. Once the HT function was applied, it can modify the contrast while suppressing highly illuminated pixels. The HT function was calculated using Eq. (2) [24].

$$I_2 = \frac{\exp(X) - \exp(-X)}{\exp(X) + \exp(-X)} \tag{2}$$

where I_2 is the resulting image from the HT function. After obtaining the two contrast-modified images, I_1 and I_2, they were combined using a suitable logarithmic image processing (LIP) method. LIP was developed initially for greyscale images, and its use was then extended to color images. LIP consists of various methods (equations) that allow the addition of two images to produce a new image that has the characteristics of both images [25]. Because the outcomes of Eqs. (1) and (2) were contrast-modified images, LIP was used to add images I_1 and I_2 together to obtain a new image that has the characteristics of both images. Different LIP addition methods exist for such purposes, in which each method produces different outcomes. To choose a suitable method, many methods were tested with different types of images. One contemporary method of interest performed reasonably well with the outcomes of the utilized S-curve functions. This LIP method could be described using Eq. (3) [26].

$$L = \sqrt[m]{1 - \frac{\left(1-I_1^m\right)\left(1-I_2^m\right)}{1-I_1^m I_2^m}} \tag{3}$$

The logarithmic model was obtained when m=1. On certain occasions, however, the resulting image can have minor contrast enhancement and a noticeable increase in brightness in some image regions. To overcome these drawbacks, Eq. (3) was adapted to the nature of the S-curve functions used. The adapted LIP method was calculated using Eq. (4).

$$L = \left(1 - \left(\frac{\left(1-I_1^2\right)\left(1-I_2^2\right)}{1-I_1^2 I_2^2} \right) \right)^4 \tag{4}$$

where L is the resulting image from the adapted LIP method. Two important goals were achieved by raising each image to the power of two and raising the entire equation to the power of four. The first was avoiding brightness amplification in the highly illuminated regions, whereas the second was providing better contrast. Another problem arose after applying Eq. (4), i.e., the brightness of the other image regions is attenuated if the brightness of highly illuminated areas is preserved.

Thus, a modified version of the probability density function of the standard Gumbel distribution (PDF-SGD) was used to improve the image brightness while preserving the brightness in the highly illuminated parts of the image. The original PDF-SGD was determined using Eq. (5) [27].

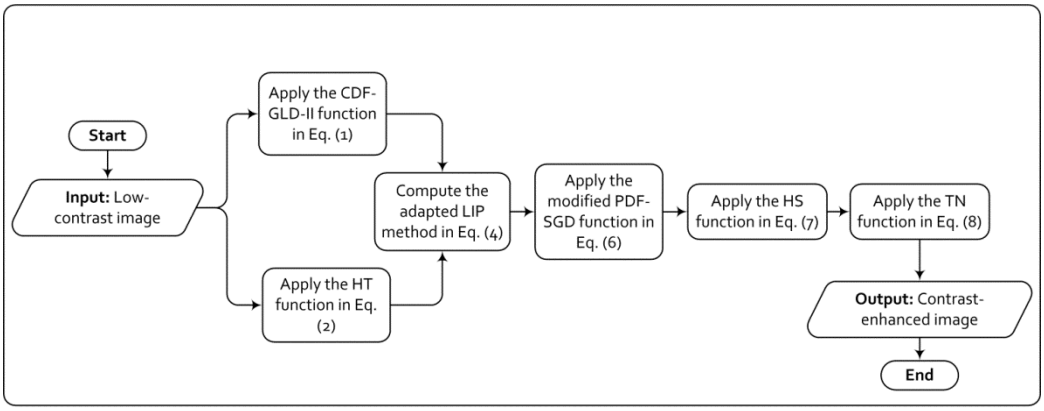

Fig. 1. Block diagram of the proposed algorithm.

$$G = \exp\left(-\left(L + \exp\left(-L\right)\right)\right) \tag{5}$$

On the other hand, if Eq. (5) is used without modification, the colors of the output image would be inverted, which means the light parts of the image become dark, and the dark parts of the image become light. To overcome such an unwanted artifact, Eq. (5) was modified heuristically to achieve the desired outcome. The modified PDF-SGD equation was determined using Eq. (6).

$$G = 1 - \exp\left(-L + \exp\left(-L\right)\right) \tag{6}$$

The resulting image G from the above equation would have the proper brightness yet slightly faded colors. Therefore, a hyperbolic sine (HS) function was applied to improve the colors of image G further. The HS function was determined using Eq. (7) [28].

$$S = \frac{\exp\left(G\right) - \exp\left(-G\right)}{2} \tag{7}$$

At this point, the contrast of the resulting image S was confined to a specific dynamic range. Therefore, a typical normalization (TN) function was applied to redistribute the image intensities into the standard dynamic range. The TN function was determined using Eq. (8) [21].

$$N = \frac{S - \min\left(S\right)}{\max\left(S\right) - \min\left(S\right)} \tag{8}$$

where N is the final output of the proposed algorithm; *max* and *min* represent the maximum and minimum pixel values of image S. The only input to the proposed algorithm was a contrast-distorted image because all calculations were conducted automatically and no other parameters were required. Fig. 1 presents the block diagram of the proposed algorithm to deliver an adequate flow and thorough explanation regarding the implementation specifics of the proposed algorithm.

3. Results and Discussion

This section reports the results of the achieved experiments and comparisons with different types of low-contrast aerial images. The aim was to deliver the required discussions regarding the findings of this research. The proposed algorithm was tested with two types of low-contrast images, i.e., artificial-degraded and natural-degraded, to determine its true processing abilities, in which the former was used in the comparisons. The latter was used in the experiments. For the utilized datasets, three publically available datasets were used in this study. The first dataset was Vehicle Detection in Aerial Imagery (VEDAI) [29], which can be found at https://downloads.greyc.fr/vedai/. This dataset consisted of 1,246 color images of different aerial scenes that were captured in unconstrained environments. The second dataset was NWPU VHR-10 [30], which can be found at http://www.escience.cn/people/JunweiHan/NWPUVHR10dataset.html. This dataset has more than 100 color remote sensing images, which also includes many aerial images that are degraded by the low-contrast effect. The third dataset was NWPU-RESISC45 [31], which can be found at http://www.escience.cn/people/JunweiHan/NWPU-RESISC45.html. This dataset contained 31,500 remote sensing images that were captured for different scenes, in which many were color aerial images that were degraded by the low-contrast effect. From these three datasets, more than 400 images were used to assess the performance of the proposed algorithm in different environments.

Fig. 2 presents a gallery of sample images that were used in this study. In addition, nine well-known and specialized contrast enhancement algorithms were used in the comparison process, i.e. WBNIE [7], BPDFHE [11], SVD_DWT [8], ESIHE [12], MMSICHE [13], HSA [14], IFAIR [9], RHEDCT [10], and HEMIC [15]. The proposed and comparison algorithms were implemented using Matlab 2018a with a computer that has 16 GB of memory and a 2.8 GHz Intel Core I7-7700HQ processor. Many specialized IQA metrics were studied for which four contemporary full-reference metrics were selected and used as an additional way to measure the quality of the attained results.

Fig. 2. Gallery of various natural-degraded color aerial images used in this study.

The IQA metrics used were detail losses and additive impairments evaluation (DLAIE) [32], sparse feature fidelity (SFF) [33], gradient magnitude similarity deviation (GMSD) [34], and multiscale contrast similarity deviation (MCSD) [35]. The DLAIE metric assesses the additive impairments and detail losses separately when evaluating an image. Detail loss denotes the loss of meaningful visual information, whereas additive impairment denotes the unnecessary information that hampers the view of useful image contents. Accordingly, a specialized decoupling method in the wavelet domain was used to separate these two features. Within this process, two important characteristics of the human visual system (HVS), which are the contrast masking effect and the contrast sensitivity, were considered to estimate the HVS sensitivities. These two characteristics were highly beneficial for detecting the amount of contrast alteration between the assessed images.

In addition, the SFF metric evaluates images utilizing the fidelity elements of its sparse features that were obtained using a specialized detector. The SFF was calculated based on two phases of fidelity computation and training. The fidelity computation involves two key elements of luminance correlation and feature similarity. The luminance correlation appraises the illumination distortions, while the feature similarity appraises the structural differences. The SFF was tested with a variety of degradations, including contrast alteration, and was found to be a highly effective quality assessment. Similarly, the GMSD metric evaluates the images based on their gradients because they are quite sensitive to distortions. This was done by exploring the utilization of the gradient's global variation for quality assessment. Accordingly, the GMSD was developed based on the pixel-wise gradient magnitude similarity (GMS) between the evaluated images pooled with the standard deviation of the GMS map to calculate the perceptual quality of the evaluated images accurately.

The gradient magnitude was used because it can describe the local image contrast precisely. Therefore, it can be an effective metric for describing the alteration of contrast between the assessed images. Moreover, the MCSD metric evaluates the contrast using its multiscale representation because it can incorporate the details of an image at various resolutions while considering the contrast relevancy to the viewing clarity. In this metric, the multiscale representation was determined iteratively using a low-pass filter and downsampling the output by a factor of two. For the assessed image at each scale, the contrast similarity deviation (CSD), which is a contrast similarity map between these two images, was computed. Finally, the determined CSDs at three scales were combined to produce the overall score.

The results of these metrics are numerical values that fall in the range of zero to one, wherein values close to one signify poor-visible quality for MCSD and GMSD but high-visible quality for DLAIE and SFF. In contrast, values close to zero signify high visible quality for MCSD and GMSD but poor visible quality for DLAIE and SFF. Figs. 3-5 show the experimental results with natural-degraded images. Figs. 6-8 present the results of the performed comparisons with the artificial-degraded images. Tables 1 and 2 list the recorded accuracies and the execution times of the achieved comparisons. The size of all images used from the VEDAI dataset in Fig. 3 was 1024×1024. The sizes of the images used from the NWPU VHR-10 dataset in Fig. 4 were 552×552, 544×544, 553×553, 760×760, 767×767, and 758×758, respectively. In addition, the size of images used from the NWPU-RESISC45 dataset in Fig. 5 was 256×256. Fig. 9 presents the graphical charts of the average scores in Tables 1 and 2.

From the obtained experimental results, the proposed algorithm provided satisfactory results when processing various natural-degraded images. The intensities of the unprocessed low-contrast images have improper distributions in the standard dynamic range. When the proposed algorithm was applied, it could provide a proper redistribution of intensities to the entire dynamic range. Therefore, the resulting images appeared with acceptable

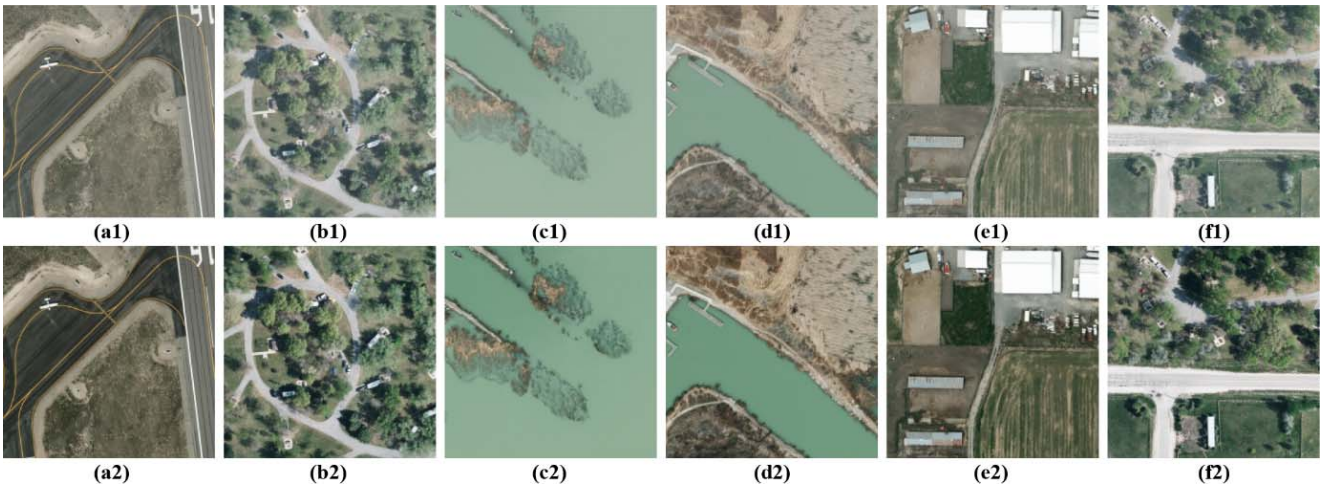

Fig. 3. Using the proposed algorithm to process different natural low-contrast images obtained from the VEDAI dataset (a1-f1) low-contrast color aerial images, (a2-f2) resulting images by the proposed algorithm.

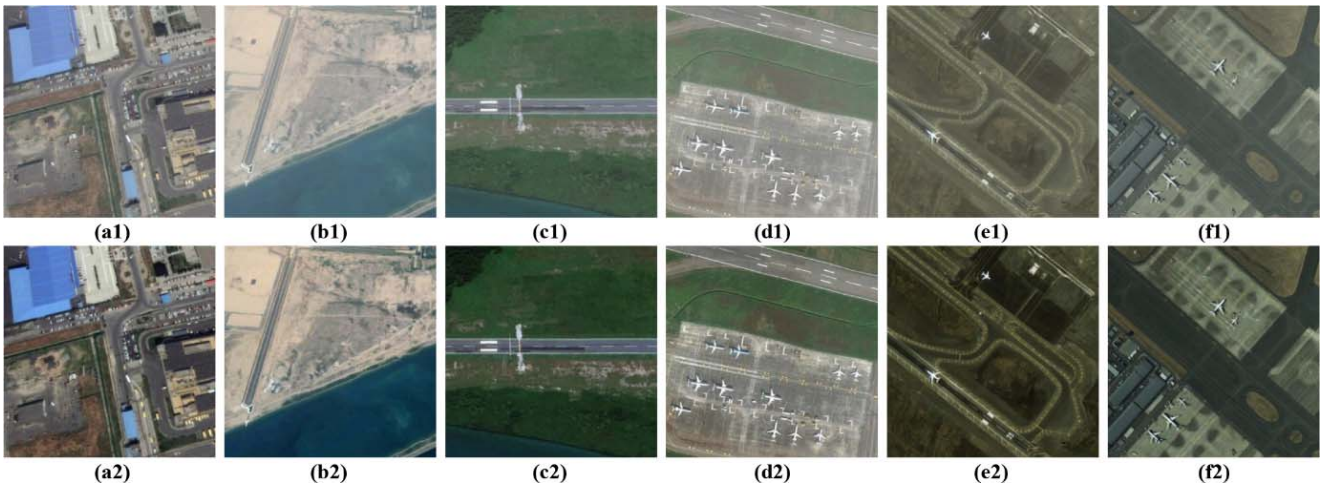

Fig. 4. Using the proposed algorithm to process different natural low-contrast images obtained from the NWPU VHR-10 dataset (a1-f1) low-contrast color aerial images, (a2-f2) resulting images by the proposed algorithm.

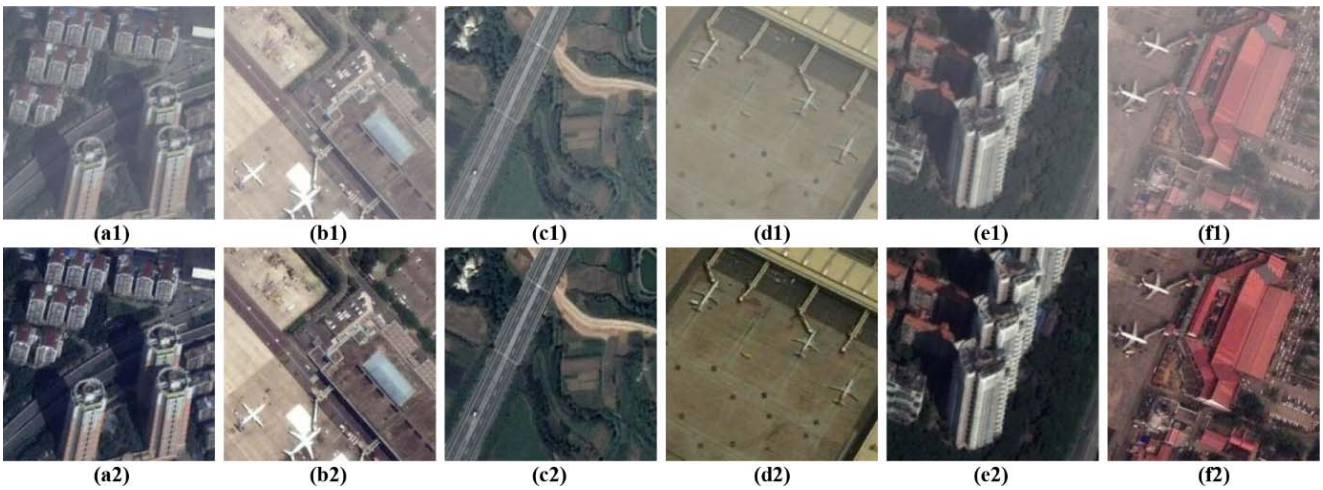

Fig. 5. Using the proposed algorithm to process different natural low-contrast images obtained from the NWPU-RESISC45 dataset (a1-f1) low-contrast color aerial images, (a2-f2) resulting images by the proposed algorithm.

Table 1. IQA scores of the achieved comparisons using images with artificial contrast reduction.

Competitors	CRR	DLAIE	SFF	GMSD	MCSD
Degraded Images	30%	0.7018	0.9874	0.0248	0.0215
	60%	0.3997	0.9313	0.0967	0.0917
	90%	0.0986	0.8418	0.3284	0.3181
	Average	*0.40003*	*0.92016*	*0.14996*	*0.14376*
WBNIE [7]	30%	0.4997	0.8294	0.1590	0.1467
	60%	0.4732	0.7845	0.1913	0.1868
	90%	0.3428	0.8389	0.3003	0.2909
	Average	*0.43856*	*0.8176*	*0.21686*	*0.20813*
BPDFHE [11]	30%	0.5185	0.9661	0.0841	0.0729
	60%	0.3038	0.7676	0.1016	0.0934
	90%	0.0785	0.5698	0.2633	0.2537
	Average	*0.30026*	*0.76783*	*0.14966*	*0.14*
SVD_DWT [8]	30%	0.8042	0.9420	0.0216	0.0185
	60%	0.6836	0.8533	0.0607	0.0424
	90%	0.1314	0.8285	0.2879	0.2795
	Average	*0.53973*	*0.8746*	*0.1234*	*0.11346*
ESIHE [12]	30%	0.9451	0.9828	0.0169	0.0160
	60%	0.8127	0.9456	0.0473	0.0446
	90%	0.5963	0.9614	0.0434	0.0418
	Average	*0.7847*	*0.96326*	*0.03586*	*0.03413*
MMSICHE [13]	30%	0.8881	0.9717	0.0222	0.0197
	60%	0.4831	0.9004	0.0846	0.0777
	90%	0.3418	0.7735	0.1782	0.1656
	Average	*0.571*	*0.88186*	*0.095*	*0.08766*
HSA [14]	30%	0.5511	0.9583	0.1378	0.1303
	60%	0.4874	0.9348	0.1067	0.1034
	90%	0.3873	0.9054	0.1052	0.0994
	Average	*0.47526*	*0.93283*	*0.11656*	*0.11103*
IFAIR [9]	30%	0.8651	0.9263	0.0396	0.0295
	60%	0.6356	0.8137	0.0469	0.0378
	90%	0.6186	0.8759	0.0551	0.0481
	Average	*0.70643*	*0.87196*	*0.0472*	*0.03846*
RHEDCT [10]	30%	0.7356	0.9658	0.0511	0.0383
	60%	0.6037	0.8943	0.0655	0.0567
	90%	0.5757	0.8217	0.1584	0.1395
	Average	*0.63833*	*0.89393*	*0.09166*	*0.07816*
HEMIC [15]	30%	0.9037	0.9841	0.0225	0.0215
	60%	0.6689	0.9649	0.0347	0.0348
	90%	0.5973	0.8804	0.0583	0.0555
	Average	*0.7233*	*0.94313*	*0.0385*	*0.03726*
Proposed Algorithm	30%	0.9714	0.9907	0.0134	0.0127
	60%	0.8892	0.9594	0.0308	0.0312
	90%	0.7615	0.9675	0.0292	0.0254
	Average	***0.87403***	***0.97253***	***0.02446***	***0.0231***

1-The best IQA scores are **boldfaced**. **2**-CRR is "Contrast Reduction Ratio".

contrast, preserved brightness, and better colors. Moreover, the results revealed adequate ability to provide visually pleasing results with no major visible flaws and no color shift, providing evidence that the proposed algorithm can process a range of low-contrast aerial images competently. This is impressive because the proposed algorithm only involved a small number of calculations to process a given image, which is unlike other algorithms that require many calculations to produce similar results. Providing natural tonality and colors for aerial images is very important. On the other hand, with the existence of numerous contrast enhancement algorithms, the provision of natural tonality and colors to processed images has become even more essential in generating valuable images. This purpose was achieved using the proposed algorithm because the results appear as if a layer of fog had been pulled from processed images while preserving the original brightness, colors, details, and structure. The obtained comparison results showed that different results are achieved. Regarding WBNIE, it performed relatively poorly, in which regions that were already bright were forced to pure white, and regions that were already dark were forced to pure black. This means losing both the highlight and shadow details. When the contrast reduction ratio was high, the colors of the processed image by this algorithm appeared slightly faded, as shown in Fig. 8(c). In terms of the IQA and execution times, it scored quite low in such traits. The BPDFHE performed somewhat poorly, in which it improved the contrast slightly in some regions, but the contrast of the processed images was still inadequate.

The worst performance was recorded when the contrast reduction ratio was high. The IQA scored low in such a trait, but it was the fastest method in terms of the execution times. The SVD_DWT provided somewhat moderate enhancement for low and medium contrast-reduced images while it provided low enhancement when the contrast reduction was high. In addition, it introduced an apparent increase in global brightness to the processed images. On the other hand, it scored somewhat moderate in terms of the IQA with fast execution times.

The ESIHE provided rich colors for the processed images with good contrast enhancement. The worst performance was recorded when the contrast reduction ratio was high. The IQA scored well in such a trait with moderate execution times. Regarding MMSICHE, it provided acceptable contrast enhancement. On the other hand, the colors of the resulting images were modified in a way that made them somewhat different from their original versions. This is why it scored moderately in terms of the IQA with the slowest execution times. The HSA modified the contrast, increased the overall brightness, and changed the colors of the processed images slightly. This is why it provided moderate IQA readings with moderate execution times.

The IFAIR performed very well in terms of contrast enhancement. On the other hand, it introduced artifacts and color shifts to the processes images. This is why it scored moderately in terms of the IQA with moderate execution times. The RHEDCT performed well in improving the contrast and preserving the brightness. On the other hand, it affected the colors of the processed images considerably

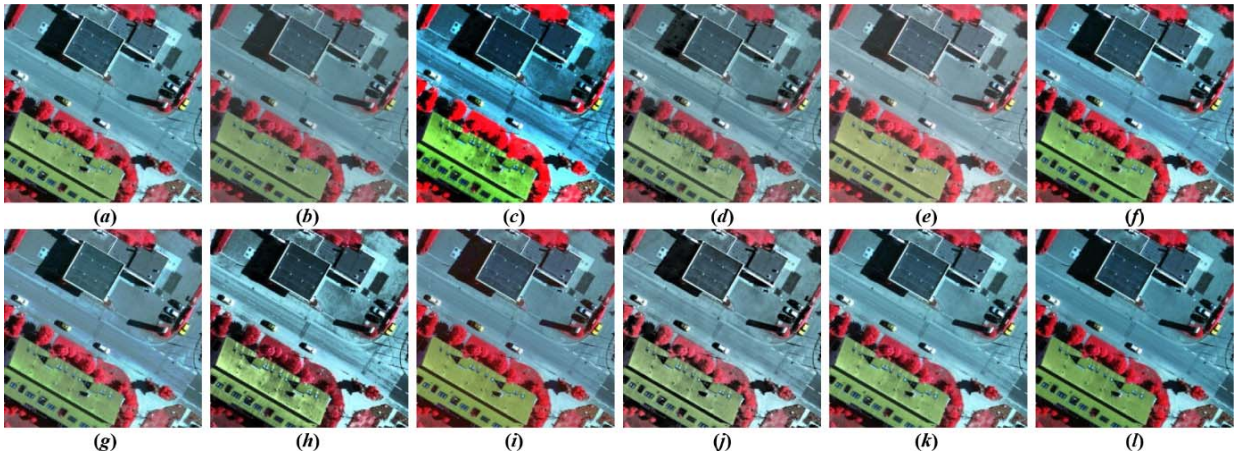

Fig. 6. Comparison results obtained by the proposed and the comparable algorithms using an artificial-degraded aerial image (a) ideal (674×674) aerial image, (b) image (a) after reducing its contrast by (30%). The rest of the images are processed by (c) WBNIE, (d) BPDFHE, (e) SVD_DWT, (f) ESIHE, (g) MMSICHE, (h) HAS, (i) IFAIR, (j) RHEDCT, (k) HEMIC, (l) proposed algorithm.

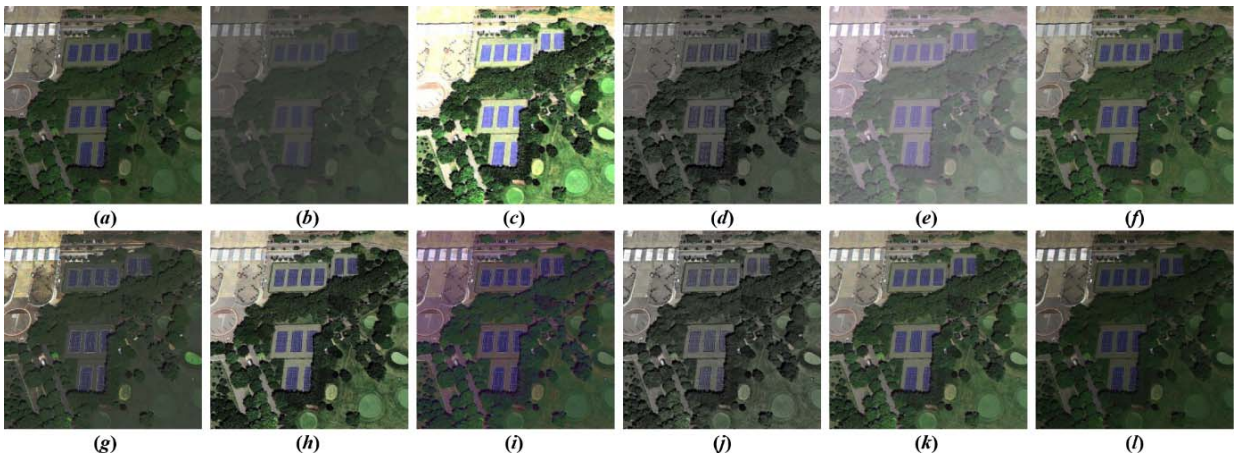

Fig. 7. Comparison results obtained by the proposed and the comparable algorithms using an artificial-degraded aerial image (a) ideal (629×629) aerial image, (b) image (a) after reducing its contrast by (60%). The rest of the images are processed by (c) WBNIE, (d) BPDFHE, (e) SVD_DWT, (f) ESIHE, (g) MMSICHE, (h) HAS, (i) IFAIR, (j) RHEDCT, (k) HEMIC, (l) proposed algorithm.

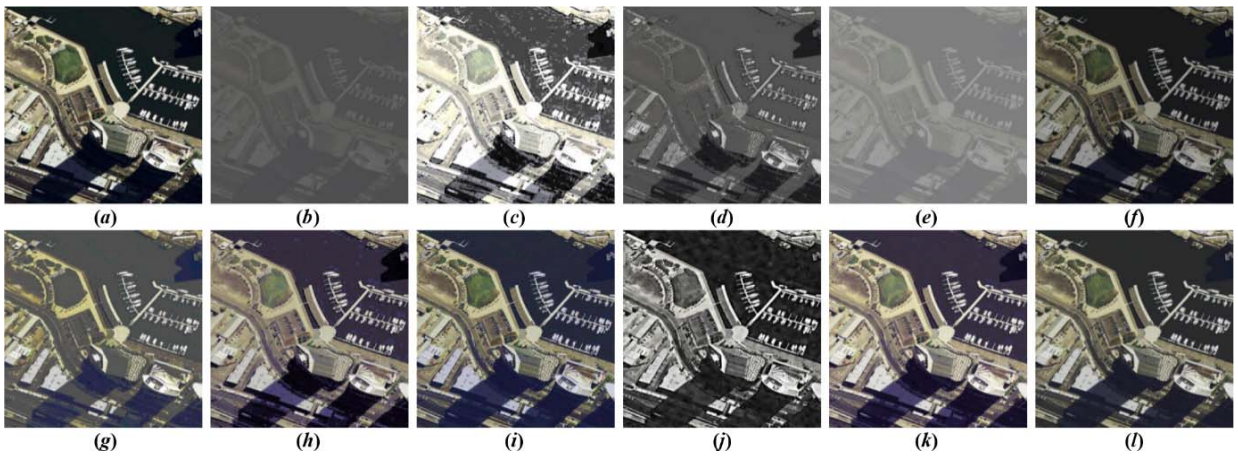

Fig. 8. Comparison results obtained by the proposed and the comparable algorithms using an artificial-degraded aerial image (a) ideal (585×585) aerial image, (b) image (a) after reducing its contrast by (90%). The rest of the images are processed by (c) WBNIE, (d) BPDFHE, (e) SVD_DWT, (f) ESIHE, (g) MMSICHE, (h) HAS, (i) IFAIR, (j) RHEDCT, (k) HEMIC, (l) proposed algorithm.

Table 2. Execution times (in seconds) for the proposed and the compared algorithms.

Algorithms	CRR 30%	CRR 60%	CRR 90%	Averages
WBNIE [7]	5.237837	3.016733	2.582447	3.612339
BPDFHE [11]	0.132181	0.096108	0.093576	0.107288
SVD_DWT [8]	0.595921	0.584962	0.506469	0.562450
ESIHE [12]	2.557378	2.185618	1.829861	2.190952
MMSICHE [13]	5.973884	5.103874	4.289655	5.122471
HSA [14]	3.736342	2.821595	2.634162	3.064033
IFAIR [9]	3.390360	2.958406	2.803504	3.050756
RHEDCT [10]	0.531314	0.452907	0.308262	0.430827
HEMIC [15]	3.611682	2.959499	2.838868	3.136683
Proposed Algorithm	0.176879	0.149741	0.134497	0.153705

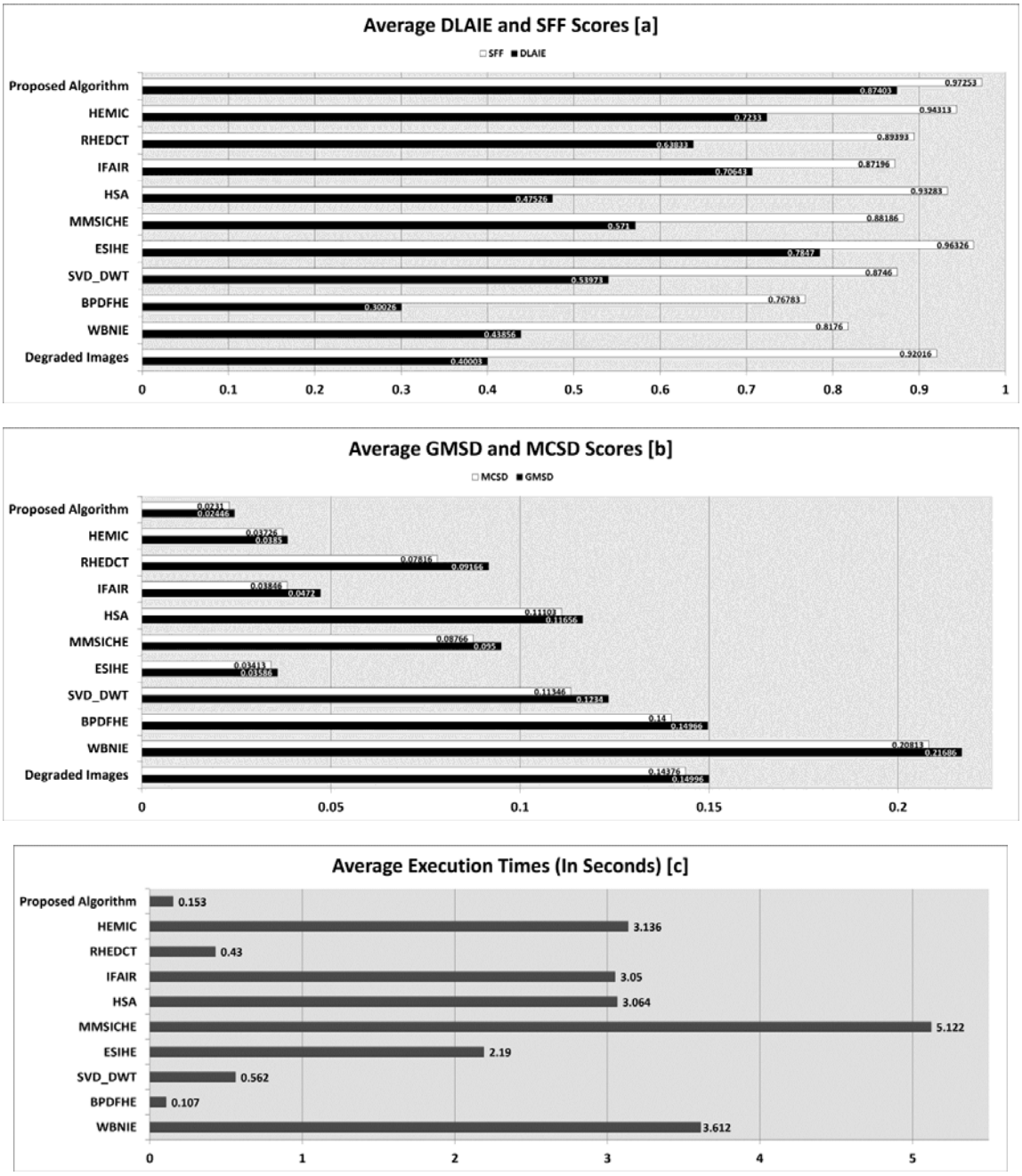

Fig. 9. Graphical representations of the average scored performances (a) DLAIE and SFF, (b) GMSD and MCSD, (c) execution times.

because they appeared in washed-out colors. This is why they did not achieve high IQA scores, but it provided fast execution times. The HEMIC performed very well in terms of contrast enhancement. On the other hand, it increased the overall brightness slightly and provided a slight color shift when processing the image with a high contrast reduction.

In addition, HEMIC provided high IQA readings, and it was very competitive with the proposed algorithm. Nevertheless, its readings did not surpass the readings of the proposed algorithm because of the mentioned downsides. This algorithm showed reasonable execution times. The proposed algorithm performed very well in all situations of contrast reduction. The algorithm provided the highest IQA readings because the resulting images were similar to the reference images. Moreover, the results showed acceptable brightness, preserved brightness, and rich colors with no visible flaws. This is significant because the results were achieved using a small number of calculations. The execution times were the second-fastest among the algorithms compared. Developing a new algorithm to improve the contrast of aerial images is a demanding task. Nevertheless, this task was achieved because the proposed algorithm was efficient with various color images and could produce visually pleasing results.

4. Conclusion

his paper proposed a new multi-concept algorithm to improve the contrast of aerial images efficiently in a fully-automatic manner by utilizing a combination of well-known processing concepts. The proposed algorithm was tested with artificial and natural-degraded low-contrast aerial images, in which the artificially degraded images were used for comparison, while the naturally degraded images were used for experimental purposes. Furthermore, the proposed algorithm was compared with nine specialized contrast enhancement algorithms, and the results of such comparisons were benchmarked with four advanced IQA metrics. From the results, the proposed algorithm performed remarkably well by providing data with fast execution times, adequate contrast, preserved brightness, and natural colors. In addition, it showed superiority over the comparison algorithms because it provided the best IQA readings. The advantages of the proposed algorithm over some modern algorithms, which include complex concepts, such as deep learning, are the low-computation cost, simplicity, ease of use, fully-automatic, and fewer variables involvement. Future studies should improve the proposed algorithm further and adapt it to other imaging applications that have contrast-distorted images, including medical, thermal, biological, satellite, microscopic, and machine vision.

Acknowledgment

The author would like to thank the authors of articles [29-31] for making their datasets available freely online. Moreover, the author wishes to acknowledge the Computer Science Department at the University of Mosul for providing true support that led to the completion of this study. In addition, the author would like to declare that this study did not receive any funding.

References

[1] T. Hinchcliffe, “Aerial photography and the postwar urban planner in london”, *The London Journal*, vol. 35, no. 3, pp. 277-288, 2010. Article (CrossRef Link)

[2] S. Chen, C. Rice, C. Boyle and E. Hauser, “Small-format aerial photography for highway-bridge monitoring”, *Journal of Performance of Constructed Facilities*, vol. 25, no. 2, pp. 105-112, 2011. Article (CrossRef Link)

[3] Y. Li and H. Wu, “Adaptive building edge detection by combining LiDAR data and aerial images”, *The International Archives of the Photogrammetry, Remote Sensing and Spatial Information Sciences*, vol. 3, no. 37, pp. 197-202, 2008. Article (CrossRef Link)

[4] P. Sidike, V. Sagan, M. Qumsiyeh, M. Maimaitijiang, A. Essa and V. Asari, “Adaptive trigonometric transformation function with image contrast and color enhancement: application to unmanned aerial system imagery”, *IEEE Geoscience and Remote Sensing Letters*, vol. 15, no. 3, pp. 404-408, 2018. Article (CrossRef Link)

[5] S. Samanta et al., “Log transform based optimal image enhancement using firefly algorithm for autonomous mini unmanned aerial vehicle: an application of aerial photography”, *International Journal of Image and Graphics*, vol. 18, no. 04, p. 1850019, 2018. Article (CrossRef Link)

[6] B. Akay and D. Karaboga, “A survey on the applications of artificial bee colony in signal, image, and video processing”, *Signal, Image and Video Processing*, vol. 9, no. 4, pp. 967-990, 2015. Article (CrossRef Link)

[7] N. Unaldi, S. Temel, V. Asari and Z. Rahman, “An automatic wavelet-based nonlinear image enhancement technique for aerial imagery”, *4th International Conference on Recent Advances in Space Technologies*, pp. 307-312, 2009. Article (CrossRef Link)

[8] H. Demirel, C. Ozcinar and G. Anbarjafari, “Satellite image contrast enhancement using discrete wavelet transform and singular value decomposition”, *IEEE Geoscience and Remote Sensing Letters*, vol. 7, no. 2, pp. 333-337, 2010. Article (CrossRef Link)

[9] N. Kwok and H. Shi, “An integrated framework for aerial image restoration”, *International Conference on Machine Learning and Cybernetics (ICMLC)*, pp. 322-327, 2015. Article (CrossRef Link)

[10] X. Fu, J. Wang, D. Zeng, Y. Huang and X. Ding, “Remote sensing image enhancement using regularized-histogram equalization and DCT”, *IEEE Geoscience and Remote Sensing Letters*, vol. 12, no. 11, pp. 2301-2305, 2015. Article (CrossRef Link)

[11] D. Sheet, H. Garud, A. Suveer, M. Mahadevappa and J. Chatterjee, “Brightness preserving dynamic fuzzy

histogram equalization", *IEEE Transactions on Consumer Electronics*, vol. 56, no. 4, pp. 2475-2480, 2010. Article (CrossRef Link)
[12] K. Singh and R. Kapoor, "Image enhancement using exposure based sub image histogram equalization", *Pattern Recognition Letters*, vol. 36, pp. 10-14, 2014. Article (CrossRef Link)
[13] K. Singh and R. Kapoor, "Image enhancement via median-mean based sub-image-clipped histogram equalization", *Optik: International Journal for Light and Electron Optics*, vol. 125, no. 17, pp. 4646-4651, 2014. Article (CrossRef Link)
[14] G. Jiang, S. Lin, C. Wong, M. Rahman, T. Ren, N. Kwok, H. Shi, Y. Yu and T. Wu, "Color image enhancement with brightness preservation using a histogram specification approach", *Optik: International Journal for Light and Electron Optics*, vol. 126, no. 24, pp. 5656-5664, 2015. Article (CrossRef Link)
[15] C. Wong, S. Liu, S. Liu, M. Rahman, S. Lin, G. Jiang, N. Kwok, H. Shi, "Image contrast enhancement using histogram equalization with maximum intensity coverage", *Journal of Modern Optics*, vol. 63, no. 16, pp. 1618-1629, 2016. Article (CrossRef Link)
[16] J. Lee and C. Chen, "Method for deciding semi-S curve for tone process of a digital color image", *US Patent*, US 6,870,955, 2005. Article (CrossRef Link)
[17] S. Chen, B. Wu, K. Bu and K. Chen, "Image enhancement method and apparatuses utilizing the same", *US Patent*, US 8,280,184, 2012. Article (CrossRef Link)
[18] C. Wen, J. Lee and Y. Liao, "Adaptive quartile sigmoid function operator for color image contrast enhancement", *In Color and Imaging Conference*, pp. 280-285, 2001. Article (CrossRef Link)
[19] H. Talebi and P. Milanfar, "Fast multilayer laplacian enhancement", *IEEE Transactions on Computational Imaging*, vol. 2, no. 4, pp. 496-509, 2016. Article (CrossRef Link)
[20] G. Deng, "An entropy interpretation of the logarithmic image processing model with application to contrast enhancement", *IEEE Transactions on Image Processing*, vol. 18, no. 5, pp. 1135-1140, 2009. Article (CrossRef Link)
[21] A. Łoza, D. Bull, P. Hill and A. Achim, "Automatic contrast enhancement of low-light images based on local statistics of wavelet coefficients", *Digital Signal Processing*, vol. 23, no. 6, pp. 1856-1866, 2013. Article (CrossRef Link)
[22] M. Yoon and S. Yang, "Apparatus and method for image contrast enhancement using RGB value", *US Patent*, US 11/371,887, 2007. Article (CrossRef Link)
[23] A. Olapade, "On negatively skewed extended generalized logistic distribution", *Kragujevac Journal of Mathematics*, vol. 27, no. 27, pp. 175-182, 2005. Article (CrossRef Link)
[24] B. Schrauwen, M. Wardermann, D. Verstraeten, J. Steil and D. Stroobandt, "Improving reservoirs using intrinsic plasticity", *Neurocomputing*, vol. 71, no. 7-9, pp. 1159-1171, 2008. Article (CrossRef Link)
[25] M. Jourlin, J. Breugnot, F. Itthirad, M. Bouabdellah and B. Closs, "Logarithmic image processing for color images", *Advances in Imaging and Electron Physics*, pp. 65-107, 2011. Article (CrossRef Link)
[26] C. Florea and L. Florea, "Logarithmic type image processing framework for enhancing photographs acquired in extreme lighting", *Advances in Electrical and Computer Engineering*, vol. 13, no. 2, pp. 97-104, 2013. Article (CrossRef Link)
[27] E. Gumbel, "The return period of flood flows", *The Annals of Mathematical Statistics*, vol. 12, no. 2, pp. 163-190, 1941. Article (CrossRef Link)
[28] X. Xiao, X. Ji and B. Lü, "The influence of turbulence on propagation properties of partially coherent sinh-Gaussian beams and their beam quality in the far field", *Optics & Laser Technology*, vol. 40, no. 1, pp. 129-136, 2008. Article (CrossRef Link)
[29] S. Razakarivony and F. Jurie, "Vehicle detection in aerial imagery: A small target detection benchmark", *Journal of Visual Communication and Image Representation*, vol. 34, pp. 187-203, 2016. Article (CrossRef Link)
[30] G. Cheng, P. Zhou and J. Han, "Learning rotation-invariant convolutional neural networks for object detection in VHR optical remote sensing images", *IEEE Transactions on Geoscience and Remote Sensing*, vol. 54, no. 12, pp. 7405-7415, 2016. Article (CrossRef Link)
[31] G. Cheng, J. Han and X. Lu, "Remote sensing image scene classification: benchmark and state of the art", *Proceedings of the IEEE*, vol. 105, no. 10, pp. 1865-1883, 2017. Article (CrossRef Link)
[32] S. Li, F. Zhang, L. Ma and K. Ngan, "Image quality assessment by separately evaluating detail losses and additive impairments", *IEEE Transactions on Multimedia*, vol. 13, no. 5, pp. 935-949, 2011. Article (CrossRef Link)
[33] H. Chang, H. Yang, Y. Gan and M. Wang, "Sparse feature fidelity for perceptual image quality assessment", *IEEE Transactions on Image Processing*, vol. 22, no. 10, pp. 4007-4018, 2013. Article (CrossRef Link)
[34] W. Xue, L. Zhang, X. Mou and A. Bovik, "Gradient magnitude similarity deviation: a highly efficient perceptual image quality index", *IEEE Transactions on Image Processing*, vol. 23, no. 2, pp. 684-695, 2014. Article (CrossRef Link)
[35] T. Wang, L. Zhang, H. Jia, B. Li and H. Shu, "Multiscale contrast similarity deviation: An effective and efficient index for perceptual image quality assessment", *Signal Processing: Image Communication*, vol. 45, pp. 1-9, 2016. Article (CrossRef Link)
[36] J. Park, J. Lee, D. Yoo and I. Kweon, "Distort-and-recover: Color enhancement using deep reinforcement learning", *2018 IEEE/CVF Conference on Computer Vision and Pattern Recognition*, pp. 5928-5936, 2018. Article (CrossRef Link)
[37] L. Zhuang and Y. Guan, "Image enhancement by deep learning network based on derived image and retinex", *2019 IEEE 3rd Advanced Information*

Management, Communicates, Electronic and Automation Control Conference (IMCEC), pp. 1670-1673, 2019. Article (CrossRef Link)

Zohair Al-Ameen was born in 1985. He received his B.Sc. degree in Computer Science from the University of Mosul in 2008. He received his M.Sc. and Ph.D. degrees in Computer Science from the Technological University of Malaysia in 2011 and 2015, respectively. He was awarded the best student award owing to the outstanding performance in his Ph.D. studies. He visited the University of Central Oklahoma, United States, for 10 weeks as a 2019 Fulbright visiting scholar. His research interest includes digital image processing (image enhancement & restoration). Currently, he works full-time at the Department of Computer Science, College of Computer Science and Mathematics, University of Mosul. He has authored many articles published in high impact international journals.